Nanoscale

RSC Publishing

PAPER

# Reactive molecular dynamics simulations on $SiO_2$-coated ultra-small Si-nanowires

Cite this: *Nanoscale*, 2013, **5**, 719

Umedjon Khalilov,*[a] Geoffrey Pourtois,[ab] Annemie Bogaerts,[a] Adri C. T. van Duin[c] and Erik C. Neyts[a]

Received 21st August 2012
Accepted 13th November 2012

DOI: 10.1039/c2nr32387g

**www.rsc.org/nanoscale**

The application of core–shell Si–$SiO_2$ nanowires as nanoelectronic devices strongly depends on their structure, which is difficult to tune precisely. In this work, we investigate the formation of the core–shell nanowires at the atomic scale, by reactive molecular dynamics simulations. The occurrence of two temperature-dependent oxidation mechanisms of ultra-small diameter Si-NWs is demonstrated. We found that control over the Si-core radius and the $SiO_x$ ($x \leq 2$) oxide shell is possible by tuning the growth temperature and the initial Si-NW diameter. Two different structures were obtained, *i.e.*, ultrathin $SiO_2$ silica nanowires at high temperature and Si core|ultrathin $SiO_2$ silica nanowires at low temperature. The transition temperature is found to linearly decrease with the nanowire curvature. Finally, the interfacial stress is found to be responsible for self-limiting oxidation, depending on both the initial Si-NW radius and the oxide growth temperature. These novel insights allow us to gain control over the exact morphology and structure of the wires, as is needed for their application in nanoelectronics.

## 1 Introduction

Small-diameter (<10 nm) Si-NWs are potentially very attractive because of the quantization of the electronic structure.[1,2] Normally, such Si-NWs are obtained by oxidizing a large nanowire and subsequently removing the oxide layer.[3–5] Such oxidation can reduce the Si-NW diameter below the Bohr exciton radius to obtain visible photoluminescence due to quantum confinement effects. Interestingly, in this case, the band gap becomes size dependent and increases as the size of the nanostructure decreases, which indicates the possibility of developing Si-NW materials with a controllable band gap.[1] For these and other applications to occur, obtaining an accurate control over the oxidation process is critical, which, however, is difficult to achieve.[6] This requires a fundamental understanding of the oxidation mechanism of such small Si-NWs, which may be significantly different from the existing mechanisms for micrometer sized Si-NWs.[7,8]

In microelectronics, self-limiting oxidation of Si nanowires and spheres at the micrometer scale is of considerable concern, for instance for the design of metal–oxide–semiconductor (MOS) devices,[2,8–14] such as wrap-gated[15] and top-gated[9] FETs or photovoltaic cells.[16] The oxidation behavior in this micrometer regime has been successfully modeled by Kao *et al.* for the case of wet Si-NW oxidation.[8] However, the oxidation behavior during dry oxidation has not yet been properly investigated. Furthermore, such studies for ultra-small diameter Si-NWs begin to appear only now.[10]

Once the self-limiting oxidation is established for small Si-NWs, the understanding of the stress dependence and the non-conservative nature of the oxidation process will be useful for controlling non-planar oxidation large scale integrated processes.[11] The residual stress results in self- (or stress-) limiting oxidation when the strain energy at the interface is larger than the energy gain for the ambient oxygen to diffuse into and oxidize the inner Si. Because the oxide should expand more to accommodate the volume expansion in thinner Si-NWs, the self-limiting oxidation is more significant in Si-NWs with smaller diameters.[11] According to the Kao model,[8] compressive stresses normal to the Si|$SiO_2$ interface reduce the interfacial reaction rate compared to a planar Si surface, whereas tensile stresses generated within the oxide shell reduce the effective oxide viscosity and enhance the oxygen diffusivity and solubility.[6] However, such stress behavior may change in the oxidation of Si-NWs at the nanoscale, as the shape of the nanowire changes accordingly from circular to polygonal with increasing curvature. Thus, stress results at the nanoscale may disagree with the conclusions for Si-NW oxidation at the micro-scale due to this "curvature effect".[17]

As mentioned above, the oxidation of ultra-small Si-NWs (<3 nm) has not yet been often studied. Various characteristics and processes, including dry oxidation mechanisms of small Si-NWs at different temperatures, self-limiting oxidation behavior, as well as the effects of size, temperature and stress on the

[a]*Department of Chemistry, PLASMANT Research Group, University of Antwerp, Universiteitsplein 1, B-2610 Wilrijk-Antwerp, Belgium. E-mail: umedjon.khalilov@ua.ac.be*

[b]*IMEC, Kapeldreef 75, B-3001 Leuven, Belgium*

[c]*Department of Mechanical and Nuclear Engineering, Penn State University, University Park, Pennsylvania 16802, USA*

oxidation process have not been properly studied yet. In this paper we therefore focus on the oxidation of ultra-small Si-NWs in order to unravel these effects during and after oxidation at the atomic scale. We will specifically discuss the ability to control the Si-core radius and oxide sheath thickness by dry thermal oxidation of (100) Si-NWs with initial diameters 1.0–3.0 nm in the temperature range of 300–1200 K.

## 2 Computational details

### ReaxFF potential

Oxidation of ultra-small Si-nanowires is studied using reactive molecular dynamics (MD) simulations, employing the Reactive Force Field (ReaxFF).[18,19]

ReaxFF is a classical force field with parameters optimized against both experimental and quantum mechanical (QM) data for reaction energies, reaction barriers and configuration energies as well as geometrical and structural data. ReaxFF accurately simulates bond breaking and bond formation processes, commonly approaching QM accuracy. Thus, ReaxFF serves as a link between QM and empirical force fields.[20] ReaxFF is based on the concept of the bond length–bond order/bond order–bond energy relationship.[21] The total system energy consists of partial energy terms related to bond energies, lone pairs, undercoordination, overcoordination, valence and torsion angles, conjugation, hydrogen bonding, as well as van der Waals and Coulomb interactions and so on.[19]

ReaxFF can currently describe tens of elements and their combinations and its generic nature ensures its applicability to a wide range of materials and processes.[22–32] In this work, we use the force field parameters employed by Buehler *et al.*[33] This force field was trained extensively against both Si and $SiO_2$ phases. Although $SiO_x$ ($x < 2.0$) suboxide phases were not included explicitly in this training set, our previous results on a planar $Si|SiO_2$ interface including these Si suboxide species were in good agreement with both experimental and DFT results.[34] A detailed description of the force field can be found elsewhere.[19,33–35]

Our choice for ReaxFF is based on the fact that it has been parameterized to describe deformations and strains[36,37] including bond breaking and formation, and its ability to accurately describe the expansion of the crystal during the oxide formation process.[38]

### Simulation details

In Fig. 1a, ideal (0 K) and thermalized (300 K and 1200 K) structures of the Si (100) nanowires (Si-NWs) with a diameter in the range 1–3 nm are shown. In Fig. 1b, the top view of the {110} and {001} facets in the 2.5 nm diameter Si-NW is illustrated. In our calculations, the nanowire diameter $d_0$ corresponds to the averaged distance between the center of mass of the wire and the positions of the surface atoms in the radial direction in the $(x,y)$ plane. A periodic boundary condition is applied along the $z$-axis, which corresponds to a unit cell length of 1 nm, to mimic an infinitely long nanowire. In reality, however, Si-NW have finite lengths, and longer than 1 nm. In order to test the "length effect" we have performed a number of test calculations for 1 nm diameter Si-NWs having different lengths (1 nm, 5 nm and 10 nm). The results showed that the oxidation mechanism is identical in all cases although the shapes are slightly different. Thus, we choose the 1 nm length Si-NW to minimize the computational time.

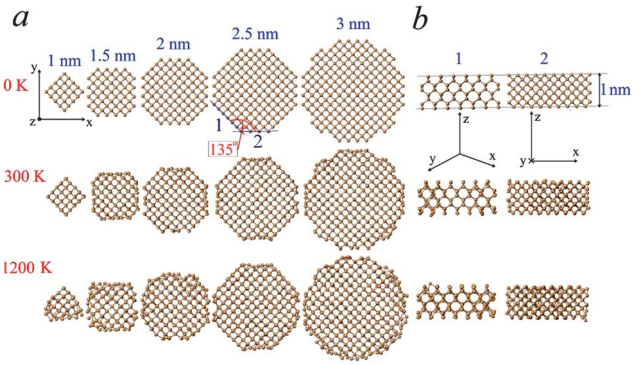


**Fig. 1** (a) Ideal (0 K) and thermalized (300 K and 1200 K) structures of Si nanowires (Si-NWs) with a diameter ($d_0$) range of 1–3 nm. The indices 1 and 2 indicate the {110} and {001}-type facets, respectively, which terminate the nanowires. (b) Top view of the facets in the Si-NW with $d_0 = 2.5$ nm at 0 K, 300 K and 1200 K, respectively.

Prior to oxidation, the ideal Si(100) NWs are equilibrated at 10 temperatures ranging from 300–1200 K in steps of 100 K for 40 ps, using the isothermal–isobaric ensemble (*i.e.*, NpT dynamics)[39] with temperature and pressure coupling parameters of 0.1 ps and 5.0 ps, respectively. We employ the NpT ensemble to ensure the generation of a zero-pressure structure at the desired temperature. To verify that the resulting structure is effectively relaxed at the desired temperature, the obtained structures are subsequently relaxed in the microcanonical NVE ensemble for another 20 ps.

The structures at low temperatures (300–700 K) display both {110} and {001} facets, similar to the ideal samples as shown in Fig. 1a. This suggested that the faceting affects the surface reaction coefficient and subsequently the oxidation rate as well.[8,13,40,41] The shapes of the NW structures at high temperatures (800–1200 K), on the other hand, become more circular (see Fig. 1a). Si–Si bond-lengths and Si–Si–Si bond angles in all structures are close to the experimental values for small Si(100) NWs.[1]

Oxygen impacts are performed as follows. Each incident oxygen molecule ($r_{O-O} = 0.121$ nm) is randomly positioned at 1 nm above the uppermost atom of the nanowire in the $(x,y)$ plane. The $O_2$ molecule is rotated randomly prior to impact. Every impact is followed for 10 ps, after which the next impact starts. The initial velocity vector of the incident molecule is randomized and its magnitude is set to the root-mean-square velocity corresponding to the oxidation temperature. During the impacts, NpT dynamics are applied to allow for a volume expansion due to the oxidation process, as mentioned above.

### Stress calculation details

During and after oxidation, Cauchy atomic stresses were calculated as the virial stress for pristine Si and the oxide

 

sheathed Si nanowires.[42] The local stress is calculated by dividing the nanowire structure into small rectangular boxes.[43] The stress tensor has 6 components for each atom and is stored as a 6-elements vector in rectangular Cartesian coordinates $(x,y,z)$: $\sigma_{xx}$, $\sigma_{yy}$, $\sigma_{zz}$, $\sigma_{yz}$, $\sigma_{zx}$, and $\sigma_{xy}$. The local tensor of each $i$ atom is defined as

$$\sigma_i = \begin{bmatrix} \sigma_{ixx} & \sigma_{ixy} & \sigma_{ixz} \\ \sigma_{iyx} & \sigma_{iyy} & \sigma_{iyz} \\ \sigma_{izx} & \sigma_{izy} & \sigma_{izz} \end{bmatrix} = \frac{1}{2\Omega} \sum_{k=1}^{N} \vec{F}_{ik} \times \vec{r}_{ik} \quad (1)$$

where $\Omega$ is the volume of the rectangular box, $\boldsymbol{F}_{ik}$ is the vector of the force acting on atom $i$ due to atom $k$, which are separated from each other by the vector $\boldsymbol{r}_{ik}$. $N$ is the total number of neighbors of atom $i$. The stresses in Cartesian coordinates are transformed into cylindrical coordinates $(r,\theta,z)$ as $\sigma_{rr}$, $\sigma_{\theta\theta}$, $\sigma_{zz}$, $\sigma_{\theta z}$, $\sigma_{zr}$, and $\sigma_{r\theta}$ as follows:[44]

$$\begin{aligned} \sigma_{rr} &= \sigma_{xx}\cos^2\theta + \sigma_{yy}\sin^2\theta + \sigma_{xy}\sin 2\theta \\ \sigma_{\theta\theta} &= \sigma_{xx}\sin^2\theta + \sigma_{yy}\cos^2\theta - \sigma_{xy}\sin 2\theta \\ \sigma_{zz} &= \sigma_{zz} \\ \sigma_{\theta z} &= \sigma_{yz}\cos\theta - \sigma_{zx}\sin\theta \\ \sigma_{zr} &= \sigma_{yz}\sin\theta + \sigma_{zx}\cos\theta \\ \sigma_{r\theta} &= (\sigma_{yy} - \sigma_{xx})\sin\theta\cos\theta + \sigma_{xy}\cos 2\theta \end{aligned} \quad (2)$$

where, $\cos\theta = \frac{x}{r}$, $\sin\theta = \frac{y}{r}$, $z = z$. The local stress in each box is calculated by averaging the atomic stresses of the atoms included in the box.

For all stress calculations, the structures were first equilibrated at 0.01 K using NpT dynamics, to remove the kinetic energy part from the stress calculation. Subsequently, the total energy was minimized using the steepest descent and conjugate gradient techniques.[45]

## 3 Temperature-dependent oxidation mechanism

The dry oxidation behavior of a 2 nm diameter ultrasmall Si-NW is illustrated in Fig. 2, showing the oxide formation and growth process of the nanowire as a function of the $O_2$ fluence at (a) low (300 K) and (b) high (1200 K) temperature. The time evolution of the formation and growth of the oxygenated silicon is studied by observing the variation of the silicon sub-oxide components ($Si^{i+}$, $i \leq 4$) in order to easily compare with experiment (*i.e.*, Si-2p photoemission spectra[46]) and validate our results.

Prior to oxidation, only $Si^0$ components are found, *i.e.*, Si–O bonds do not exist in the Si-NW (Fig. 2, initial structures). When the oxidation process starts, only $Si^{1+}$ and $Si^{2+}$ are initially formed. As the oxidation progresses, these are transformed into $Si^{3+}$ and subsequently into $Si^{4+}$. Note that the notation used corresponds to the formal charge states and not to the actual atomic charges. Our calculations show that the $Si^{1+}$, $Si^{2+}$, and $Si^{3+}$ fractions consecutively dominate in the initial oxidation stage. In this stage, the oxygenated Si-NW consists of crystalline silicon (*c*-Si) and a $SiO_x$ region. After a fluence of 2 ML (Fig. 2), the $Si^{4+}$ suboxide species are also found on the oxidized Si-NW at low temperature, but not yet at high temperature. This means that the consecutive $Si^{1+} \rightarrow Si^{2+} \rightarrow Si^{3+} \rightarrow Si^{4+}$ conversion (*i.e.*, the appearance of a new silica layer) occurs much faster at low temperature than at high temperature. Indeed, at low temperature, the penetrated O atoms or molecules cannot move deeper into the nanowire due to the associated energy barrier and the Si–Si bonds convert relatively fast into Si–O bonds in the $SiO_x$ region. When a stoichiometric ($SiO_2$) oxide layer appears, the fraction of $Si^{4+}$ components increases continuously and the fractions of the other suboxide components therefore decrease, as is clear from Fig. 2. This indicates the end of the initial oxidation stage. Our simulations show that this stage ends earlier at low temperature than at high temperature.

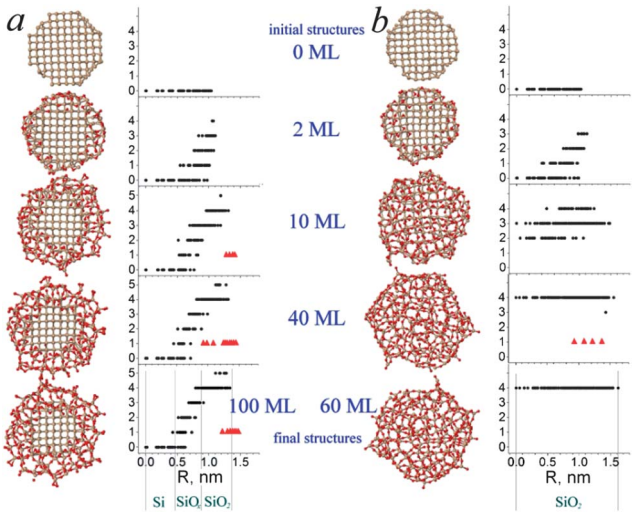


**Fig. 2** Oxide formation and growth as a function of the $O_2$ fluence in the 2 nm Si-NW at (a) low (300 K) and (b) high (1200 K) temperature, respectively. 1 ML corresponds to 28 $O_2$. Each structure is analyzed by the radial distribution of the Si-(sub)oxide components (black circles) and the O–O peroxyl bridges (red triangles). $R$ is the radial distance from the centre of the Si-NW (*i.e.*, $R = 0$) to the nanowire atoms in the $(x,y)$ plane. Here, Si, $SiO_x$, $(x > 2)$ and $SiO_2$ correspond to the crystalline silicon (or Si-core), non-stoichiometric oxide and amorphous silica regions, respectively.

In the stage between 2 ML and 10 ML, the oxide growth process at low temperature is almost entirely stopped due to the energy barrier, interfacial stresses and lowered diffusivity of the penetrated oxygen species. This also leads to the appearance of some overcoordinated silicon ($Si^{5+}$) species in the $SiO_2$ region,[10,47] albeit at low concentration (see Fig. 2a). The silica contains a number of O–O peroxyl bonds as well (see Fig. 2, red triangles),[48] which also play a role in the appearance of $Si^{5+}$ in the oxygenated Si-NW. A similar effect was also suggested by DFT calculations by analyzing various defects during planar Si oxidation.[34,47,49,50]

Starting from 10 ML, the number of peroxyl linkages and five-fold coordinated silicon atoms increases and they spread in the whole silica region. This indicates that Si-NW oxidation is only continued by diffusing oxygen species. Therefore, the duration of this process is much longer than the initial oxidation stage. Indeed, the oxidation rate not only depends on the surface reaction coefficient, but also on the transfer and diffusion coefficients. Such an oxidation behavior is also explained in depth by Kao and co-workers in their micro-scale model.[8] Furthermore, distribution of the O–O peroxyl bridges in the Si-NW at low temperature indicated that oxidation continues in

the slow oxidation stage (see 10 and 40 ML in Fig. 2a). Such an oxidation behaviour was not reported in wet oxidation of Si-NWs.[8] A similar oxidation behaviour is also observed at high temperature (40 ML, Fig. 2b), albeit its contribution is small compared with the low temperature case. Although the oxide growth continues, the Si-core radius remains constant at low temperature after 40 ML. At high temperature, some oxygen species penetrate into the Si-NW center already at 10 ML. In the final oxidized nanowire (Fig. 2b, 100 ML), all Si atoms are in the $Si^{4+}$ oxidation state and all O–O peroxyl bridges disappear. On the other hand, at low temperature, all Si-suboxide components (including some $Si^{5+}$) can be found in the final structure after 100 ML, as is illustrated in Fig. 2a. However, such intermediate structures, *i.e.*, overcoordinated Si atoms and peroxyl linkages, are only found on the silica surface, and not in the whole silica region, indicating that the oxide growth by diffusing oxygen species has entirely stopped.

Finally, at the end of the oxidation process, two different structures are obtained (Fig. 2, final structures). The overall spread in the radial distribution function (RDF), angle and mass density distributions confirms that the initially crystalline silicon (*c*-Si) nanowire converts into either a silicon-silica (*c*-Si|$SiO_x$|*a*-$SiO_2$) nanowire at a low temperature (300 K) or an amorphous silica (*a*-$SiO_2$) nanowire at a high temperature (1200 K). This was also reported in our previous work, as well as in the literature.[10,51] The formation of the structure obtained at low temperature can be explained by self-limiting oxidation,[8,11] as will be further explained below.

## 4 Ultra-small Si|$SiO_x$|$SiO_2$ nanowires

As mentioned in the previous section, and as illustrated in Fig. 3, two types of nanostructures are ultimately obtained, *i.e.*, *c*-Si|$SiO_x$|*a*-$SiO_2$ (typical at low temperatures) and *a*-$SiO_2$ nanowires (typical at the higher temperatures). Only the 1 nm diameter Si-NW (not shown in Fig. 3) completely converts into the *a*-$SiO_2$ nanowire at all temperatures. In Fig. 3a, all finally obtained core shell *c*-Si|$SiO_x$|*a*-$SiO_2$ structures are shown. At temperatures above 800 K, all obtained structures are fully amorphous and are therefore not shown. The figure illustrates

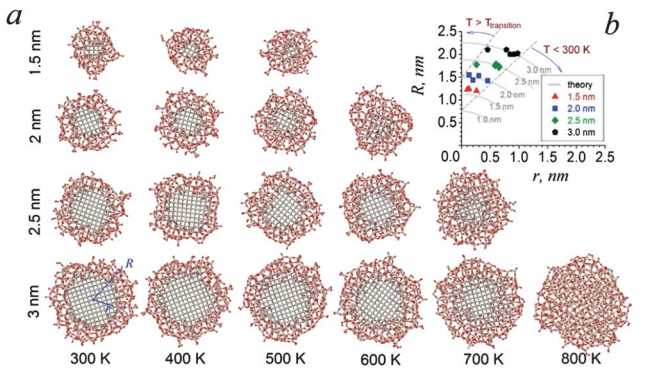


**Fig. 3** (a) The *c*-Si|$SiO_x$|*a*-$SiO_2$ nanowires with initial diameters in the range 1.5–3 nm after oxidation at $T = 300$–800 K. (b) Final radii of Si-core ($r$) and Si-NW ($R$), compared with theoretical calculations derived from eqn (3).

that both the Si-core radius ($r$) as well as the Si-NW radius ($R$) depend on the $d_0$ diameter and inversely depend on the oxidation (or oxide growth) temperature $T$, *i.e.*, $r(\text{or } R) \sim \frac{d_0}{T}$. We found that the maximum radius of the Si-core is about 0.26 nm, 0.46 nm, 0.65 nm and 0.91 nm for 1.5, 2, 2.5 and 3 nm diameter Si-NWs, respectively, at 300 K. Due to the increasing diffusivity and mobility of the penetrated oxygen atoms, the core radius drops with rising temperature. While the growth temperature increases, the Si-core radius decreases to zero ($r \rightarrow 0$) and consequently the nanowire converts into a pure $SiO_x$ ($x \leq 2$) nanowire at a certain "transition temperature" ($T_{trans}$). Thus, for a given nanowire diameter, $T_{trans}$ is the temperature above which amorphous silica (*a*-$SiO_2$) is obtained, and below which core–shell *c*-Si|$SiO_x$|*a*-$SiO_2$ nanowires are obtained. From Fig. 3a it can be seen that $T_{trans}$ is roughly equal to 500 K, 600 K, 700 K and 800 K for Si-NWs with diameters of 1.5 nm, 2 nm, 2.5 nm and 3 nm, respectively. This clearly demonstrates that control over the Si-core radius is possible by selecting the appropriate initial diameter of the Si-NW and the growth temperature.

The final radii of the *c*-Si|$SiO_x$|*a*-$SiO_2$ nanowires, as obtained in our MD calculations, can be compared with a theoretical derivation, to which also most experimentalists compare their results:[9,40,51]

$$\pi\left(R^2 - r^2\right) L - \pi\left({R_0}^2 - {r_0}^2\right) L = \frac{\Omega_{SiO_2}}{\Omega_{Si}} \pi\left({r_0}^2 - r^2\right) L \qquad (3)$$

where $r_0$, $r$ and $R_0$, $R$ are the initial and final radii of the Si-core and oxidized Si-NW, respectively; $L$ is the Si-NW length; $\Omega_{SiO_2}$ is the molecular volume of $SiO_2$ (~45 Å$^3$) and $\Omega_{Si}$ is the atomic volume of Si (20 Å$^3$). Prior to oxidation, initially $r_0 = R_0$. From (3), the following formula including this initial condition can be obtained:

$$R = \sqrt{2.25{r_0}^2 - 1.25r^2} \qquad (4)$$

The relationship between the final Si-NW ($R$) and Si-core ($r$) radii for partially oxidized structures can be calculated by means of this formula. The results are presented in Fig. 3b (grey curves). It can be seen in the figure that most of our MD results are fairly close to this theoretical calculation. Furthermore, this indicates that at low temperature, the oxidation process does not strongly depend on the diffusion coefficient and is only a function of the surface reaction rate, which depends on the normal stress rather than on the temperature. Especially in the cases above 2 nm diameter, this effect clearly appears: at all temperatures below the transition temperature, the diamonds ($d_0 = 2.5$ nm) or pentagons ($d_0 = 3$ nm) are close to each other, close to the lower dotted line, indicating that the oxidation hardly changes between these temperatures. Increasing the temperature to above the transition temperature, however, results in a strong increase in the oxidation, as indicated by the datapoints lying close to the upper dotted line. Note that this effect is not observed in the Si-NWs with a higher curvature ($d_0 < 2.5$ nm).

Indeed, it was previously suggested that compressive stresses at the Si|$SiO_2$ interface significantly slow down the reaction rate,[8,11–13] and furthermore, that a compressive pressure in $SiO_2$ can reduce the oxidant diffusion and transport.[12]

 

## 5 Stress evolutions during self-limiting oxidation

We first calculated the stresses (normal or radial $\sigma_{rr}$, tangential $\sigma_{\theta\theta}$ and axial $\sigma_{zz}$) in the pristine Si-NWs. Our calculations show that although all pre-oxidation stresses change depending on the crystal orientation and nanowire curvature, their values are very small and close to the previously suggested values.[8] Although the average values of the $\sigma_{rr}$ and $\sigma_{\theta\theta}$ stresses are compressive, their contributions to reducing the Si–O reaction rate are negligible.

In Si-NW oxidation, two key factors can be discerned: (1) oxygen diffusion in the $SiO_x$ ($x \leq 2$) oxide region, characterized by the diffusion constant $D$; and (2) reaction with the Si-core, characterized by the reaction rate constant $k_s$.[8] These two parameters also strongly depend on the hydrostatic pressure $p$ (*i.e.*, the obtained oxide can be considered as a fluid with high viscosity[8]) and the normal stress $\sigma_{rr}$ at a given temperature, respectively. According to fluid mechanics, the pressure is equal to the average total $\sigma_{rr}$ on a control volume in the fluid and it is found as $p = -\frac{1}{2}(\sigma_{rr} + \sigma_{\theta\theta})$.[52]

Fig. 4 presents the normal stress and (hydrostatic) pressure evolution during oxidation for a Si NW with $d_0 = 2$ nm at 300 K. The compressive stress (or pressure) is presented as a positive value and the tensile stress (or pressure) as a negative value. Our calculations show that in the initial oxidation stage (0–2 ML), $\sigma_{rr}$ and $p$ are tensile on average and fluctuate around 0 GPa. This permits oxygen to react easily with the Si-crystal after diffusing through the $SiO_x$ region. As a result, the oxidation rate rapidly increases in this oxidation stage. Because of the increasing reaction rate, the stress in the Si-core initially increases slightly. In this period, the oxygen atom or molecule penetrates deeper into the crystal, depending on the energy barrier of the Si surface and sub-surfaces. Consequently, the consecutive $Si^{1+} \rightarrow Si^{2+} \rightarrow Si^{3+} \rightarrow Si^{4+}$ conversion leads to a gradual expansion of the Si crystal. Specifically, when the oxide layer becomes continuous, the volume expansion resulting from the silicon oxidation is restrained by the silicon itself. This is similar to the compressive stress resulting from epitaxial growth of a film with a lattice parameter larger than the substrate.[51] When a $SiO_2$ oxide layer appears (after 2 ML) the oxygen diffusivity significantly decreases due to compressive $\sigma_{rr}$ and $p$ and the reaction rate is drastically reduced. It is also theoretically suggested that a compressive $p$ reduces the solubility of the oxygen molecule in $SiO_2$ as it raises the potential energy of the molecule in its interstitial site, whereas a tensile $p$ increases its solubility for the opposite reason.[12] Indeed, such compressive $p$ and $\sigma_{rr}$ may also significantly reduce the oxidant transport in the oxide region.

When the slow oxidation stage starts (2–10 ML), the nanowire can be divided into three parts (see Fig. 2 above): a crystalline Si-core (*c*-Si), a partially oxidized Si region ($SiO_x$, $x < 2$) and a fully oxidized Si or silica ($SiO_2$) region. It is clear from Fig. 4 that the $\sigma_{rr}$ is tensile in the $SiO_x$ ($x < 2$) oxide and at the $SiO_2$ surface, whereas it is compressive in the $SiO_2$ bulk and at the *c*-Si|$SiO_x$ interface in the slow oxidation stage (*i.e.*, ~10 ML). Note that the oxygen contribution in the stress calculation may affect the image clarity of the stress distribution in the non-stoichiometric oxide region where somewhat higher tensile stresses appear. Nevertheless, the oxygen reaction rate is high and this indicates that the stress in this region should be tensile rather than compressive. On the other hand, at the interface, the compressive normal stress gradually increases from 1.6 GPa to 2.0 GPa and 3.0 GPa after 10 ML, 40 ML and 100 ML, respectively. Finally, the Si-core stress decreases again while the interfacial stress is constant at about 3 GPa as shown in Fig. 4 (100 ML). Some classical continuum analysis concluded that such compressive stress in the silicon core significantly slows down the oxidation.[8,12,14]

## 6 Interfacial stresses

The self-limiting behavior of the Si-NW oxidation strongly depends on the aforementioned "interfacial stresses",[12–14,53] which correspond to the stresses in the outer Si shell and the oxide shell near the Si|$SiO_x$ interface. The interfacial stresses, which can also be thought of as a combination of chemical and mechanical (physical) stresses,[54] play an important role in the reliability of gate oxides with its ultrathin interface.[55]

Fig. 5 shows the interfacial stress as a function of the initial Si-NW diameter and the oxidation temperature. Our calculations predict that when the temperature increases the stress decreases. As shown in Fig. 5b, the average values of the residual stresses at the interface are 3.2 GPa, 3.0 GPa, 2.6 GPa, 2.2 GPa, and 2.04 GPa at 300 K, 400 K, 500 K, 600 K and 700 K, respectively, for the 2.5 nm Si-NW. Such a temperature dependent behavior of the interfacial stress is consistent with previous theoretical work of Si-NW oxidation.[8] The same authors also proposed that the stress is higher for smaller radii and they explained that the deformation of a small structure requires more rearrangement. However, our nanowires are all

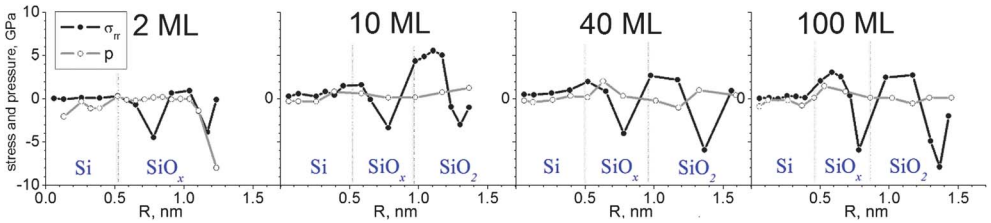


**Fig. 4** Normal ($\sigma_{rr}$) stress and hydrostatic pressure ($p$) as a function of the oxidation time for the Si-NW with $d_0 = 2$ nm at 300 K. Here, Si, $SiO_x$, ($x > 2$) and $SiO_2$ correspond to the crystalline silicon (or Si-core), non-stoichiometric oxide and amorphous silica regions, respectively.

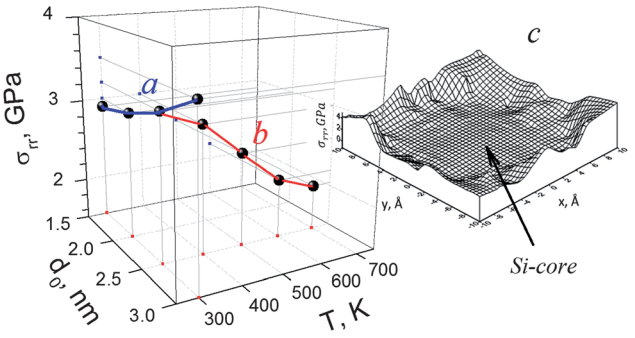


**Fig. 5** Averaged radial (normal) $\sigma_{rr}$ stresses at the Si|$SiO_2$ interface of the final oxidized Si-NW structure as a function of (a) the curvature and (b) oxide growth temperature. (c) The interfacial $\sigma_{rr}$ stress on the $x$–$y$ plane for a Si-NW with $d_0 = 3$ nm at 300 K. The (0, 0) position corresponds to the Si-NW center.

very small and the obtained results are opposite to this theoretical suggestion. Indeed, our calculations predict that the 1.5 nm diameter Si-NW exhibits a somewhat smaller compressive stress than the other nanowires (Fig. 5a). To be exact, the averaged interfacial stress of the NWs at 300 K is calculated to be 2.9 GPa, 3.0 GPa, 3.2 GPa, and 3.5 GPa for the NWs with 1.5 nm, 2 nm, 2.5 nm and 3 nm diameter, respectively. This phenomenon of a residual compressive stress decreasing with rising curvature was also reported by Kim *et al.*[17] Following these authors, the non-oxidized Si-core of smaller Si-NWs with diameters in the sub-10 nm range deforms more to compensate for the volume expansion of the surface oxide layer, resulting in a smaller compressive stress. Furthermore, we also suggest that crystal orientation effects may play a role to develop this phenomenon.

The distribution of interfacial stresses around the Si-core in the ($x$,$y$) plane is also presented in Fig. 5c. As shown in the figure, the compressive interfacial stresses at room temperature are significantly higher than the stresses of its Si-core. Such compressive stresses significantly reduce the oxygen reaction with Si near the planar Si|$SiO_2$ interface, which was investigated using high-resolution transmission electron microscopy (HRTEM) analysis.[56] Indeed, these residual stresses are relatively high at a low temperature (*e.g.*, 300 K) in ultra-small Si-NWs and therefore their effect is significant in self-limiting oxidation.[10,11] Thus, it is observed from our calculations that accurate control of the interfacial stress by choosing a suitable temperature and Si-NW diameter can lead to accurate control over the Si-core radius at the nanoscale.

## 7 Conclusions

Oxidation of ultra-small Si nanowires with initial diameters in the range 1 nm to 3 nm was studied using reactive molecular dynamics. We studied the temperature-dependent dry oxidation mechanism of small Si-NWs at low (300 K) and high (1200 K) temperatures. The oxidation mechanism is discussed in comparison to wet oxidation of micrometer sized Si-NWs and other mechanisms of planar Si oxidation. Diffusion of O–O bridge linkages is also discussed. Although their contribution is small, they may play a role in a diffusion-dependent oxidation process.

At the end of the oxidation two types of structures are found: at low temperatures, $c$-Si|$SiO_x$|$a$-$SiO_2$ nanowires are formed, while $a$-$SiO_2$ nanowires are formed at higher temperatures. The transition temperature between both regimes was found to increase with the NW diameter. Indeed, for the 1.5 nm, 2 nm, 2.5 nm and 3 nm diameter Si-NWs, the transition temperature was found to be about 500 K, 600 K, 700 K and 800 K, respectively. The final radii of the $c$-Si|$SiO_x$|$a$-$SiO_2$ nanowires are close to the theoretically suggested radii. Our calculations predict for the partially oxidized $c$-Si|$SiO_x$|$a$-$SiO_2$ nanowires that the Si-core ($c$-Si) and the total nanowire radius depend on the initial Si-NW diameter and inversely depend on the oxidation temperature.

Stress calculations were also performed to study the self-limiting nature of the oxidation of these ultra-small nanowires. It is found that a compressive pressure and stress may significantly reduce the oxidant transport in the oxide region and its reaction with the Si-core. Stresses at the interface were also analyzed. Specifically, when the temperature increases, the interfacial stresses decrease. This is consistent with previous theoretical work. However, we also found that the compressive interfacial stresses decrease with increasing curvature for the 1–3 nm Si-NWs investigated, which is in contrast to the theoretical suggestions for Si-NWs at the micro-scale.

Generally, we can conclude from our simulations that an accurate control over the interfacial stress by choosing a suitable oxidation temperature and a Si-NW diameter can lead to a precise control over the Si-core radius at the nanoscale regime.

## Acknowledgements

U. Khalilov acknowledges imec for financial support. G. Pourtois acknowledges support from the Future and Emerging Technologies (FET) program within the 7th Framework Program for Research of the European Commission under the FET-Open grant number 270749- 2DNANOLATTICES. A. C. T. van Duin acknowledges funding from the Air Force Office of Scientific Research (AFOSR) under Grant no. FA9550-10-1-0563. The authors also gratefully acknowledge financial support from the Prime Minister's Office through IAP VI. This work was carried out using the Turing HPC infrastructure at the CalcUA core facility of the Universiteit Antwerpen (UA), a division of the Flemish Supercomputer Center VSC, funded by the Hercules Foundation, the Flemish Government (department EWI) and the UA.

## References

1 D. D. D. Ma, C. S. Lee, F. C. K. Au, S. Y. Tong and S. T. Lee, *Science*, 2003, **299**, 1874.
2 K. Trivedi, H. Yuk, H. C. Floresca, M. J. Kim and W. Hu, *Nano Lett.*, 2011, **11**, 1412–1417.
3 J. S. Judge, *J. Electrochem. Soc.*, 1971, **118**, 1772–1775.
4 P. A. M. van der Heide, M. J. Baan Hofman and H. J. Ronde, *J. Vac. Sci. Technol., A*, 1989, **7**, 1719–1723.
5 J. Magyar, A. Sklyarov, K. Mikaylichenko and V. Yakovlev, *Appl. Surf. Sci.*, 2003, **207**, 306–313.

 

6 S. Krylyuk, A. V. Davydov, I. Levin, A. Motayed and M. D. Vaudin, *Appl. Phys. Lett.*, 2009, **94**, 063113.
7 B. E. Deal and A. S. Grove, *J. Appl. Phys.*, 1965, **36**, 3770–3778.
8 D.-B. Kao, J. P. McVittie, W. D. Nix and C. K. Saraswat, *IEEE Trans. Electron Devices*, 1988, **35**, 25–37.
9 B. Liu, Y. Wang, T. Ho, K.-K. Lew, S. M. Eichfeld, J. M. Redwing, T. S. Mayer and S. E. Mohney, *J. Vac. Sci. Technol., A*, 2008, **26**, 370.
10 U. Khalilov, G. Pourtois, A. C. T. van Duin and E. C. Neyts, *Chem. Mater.*, 2012, **24**, 2141–2147.
11 H. I. Liu, D. K. Biegelsen, N. M. Johnson, F. A. Ponce and R. F. W. Pease, *J. Vac. Sci. Technol., B*, 1993, **11**, 6.
12 J. Dalla Torre, J.-L. Bocquet, Y. Limoge, J.-P. Crocombette, E. Adam and G. J. Martin, *J. Appl. Phys.*, 2002, **92**, 2.
13 P.-F. Fazzini, C. Bonafos, A. Claverie, A. Hubert, T. Ernst and M. Respaud, *J. Appl. Phys.*, 2011, **110**, 033524.
14 Y. Chen, Modeling of the Self-Limiting Oxidation for Nanofabrication of Si, in *Technical Proceedings of the Third International Conference on Modeling and Simulation of Microsystem*, Nano Science and Technology Institute: Austin, TX, San Diego, CA, March 27–29, 2000, vol. 2000, pp. 56–58.
15 J. Goldberger, A. I. Hochbaum, R. Fan and P. Yang, *Nano Lett.*, 2006, **6**, 2006.
16 M. Konagai, *Jpn. J. Appl. Phys.*, 2011, **50**, 030001.
17 B.-H. Kim, M. A. Pamungkas, M. Park, G. Kim, K.-R. Lee and Y.-C. Chung, *Appl. Phys. Lett.*, 2011, **99**, 143115.
18 A. C. T. van Duin, S. Dasgupta, F. Lorant and W. A. Goddard III, *J. Phys. Chem. A*, 2001, **105**, 9396–9409.
19 A. C. T. van Duin, A. Strachan, S. Stewman, Q. Zhang, X. Xu and W. A. Goddard III, *J. Phys. Chem. A*, 2003, **107**, 3803–3811.
20 M. J. Buehler, *J. Comput. Theor. Nanosci.*, 2006, **3**, 603–623.
21 G. C. Abell, *Phys. Rev. B: Condens. Matter Mater. Phys.*, 1985, **31**, 6184–6196.
22 E. C. Neyts, Y. Shibuta, A. C. T. van Duin and A. Bogaerts, *ACS Nano*, 2010, **4**, 6665–6672.
23 E. C. Neyts, A. C. T. van Duin and A. Bogaerts, *J. Am. Chem. Soc.*, 2011, **133**, 17225–17231.
24 E. C. Neyts, A. C. T. van Duin and A. Bogaerts, *J. Am. Chem. Soc.*, 2012, **134**, 1256–1260.
25 P. Valentini, T. E. Schwartzentruber and I. Cozmuta, *J. Chem. Phys.*, 2010, **133**, 084703.
26 J. E. Mueller, A. C. T. van Duin and W. A. Goddard III, *J. Phys. Chem. C*, 2010, **114**, 5675–5685.
27 N. Ning, F. Calvo, A. C. T. van Duin, D. J. Wales and H. Vach, *J. Phys. Chem. C*, 2009, **113**, 518–523.
28 J. C. Fogarty, H. M. Aktulga, A. Y. Grama, A. C. T. van Duin and S. Pandit, *J. Chem. Phys.*, 2010, **132**, 174704.
29 K. Chenoweth, A. C. T. van Duin and W. A. Goddard III, *J. Phys. Chem. A*, 2008, **112**, 1040–1053.
30 O. Rahaman, A. C. T. van Duin, W. A. Goddard III and D. J. Doren, *J. Phys. Chem. B*, 2011, **115**, 249–261.
31 S. Monti, A. C. T. van Duin, S.-Y. Kim and V. Barone, *J. Phys. Chem. C*, 2012, **116**, 5141–5150.
32 R. M. Abolfath, A. C. T. van Duin and T. Brabec, *J. Phys. Chem. A*, 2011, **115**, 11045.
33 M. J. Buehler, A. C. T. van Duin and W. A. Goddard III, *Phys. Rev. Lett.*, 2006, **96**, 095505.
34 U. Khalilov, E. C. Neyts, G. Pourtois and A. C. T. van Duin, *J. Phys. Chem. C*, 2011, **115**, 24839–24848.
35 A. C. T. van Duin, J. M. A. Baas and B. van de Graaf, *J. Chem. Soc., Faraday Trans.*, 1994, **90**, 2881–2895.
36 Y. Park, H. M. Atkulga, A. Grama and A. Strachan, *J. Appl. Phys.*, 2009, **106**, 034304.
37 P. Ganster, G. Treglia and A. Saul, *Phys. Rev. B: Condens. Matter Mater. Phys.*, 2010, **81**, 045315.
38 A. P. Garcia, D. Sen and M. J. Buehler, *Metall. Mater. Trans. A*, 2011, **42**, 3889–3897.
39 H. J. C. Berendsen, J. P. M. Postma, W. F. van Gunsteren, A. DiNola and J. R. Haak, *J. Chem. Phys.*, 1984, **81**, 3684–3690.
40 D. Shir, B. Z. Liu, A. M. Mohammad, K. K. Lew and S. E. Mohney, *J. Vac. Sci. Technol., B*, 2006, **24**, 1333.
41 J. L. Liu, Y. Lu, Y. Shi, S. L. Gu, R. L. Jiang, F. Wang, H. M. Bu and R. L. Zheng, *Phys. Status Solidi A*, 1998, **168**, 441.
42 I. Daruka, A.-L. Barabási, S. J. Zhou, T. C. Germann, P. S. Lomdahl and A. R. Bishop, *Phys. Rev. B: Condens. Matter Mater. Phys.*, 1999, **60**, R2150–R2153.
43 H. Ohta, T. Watanabe and I. Ohdomari, *Jpn. J. Appl. Phys.*, 2007, **46**, 3277–3282.
44 I. Okumura, *On the Stress Field in Orthogonal Curvilinear Coordinates*, Memoirs of the Kitami Institute of Technology, 2000, vol. 32, pp. 51–65.
45 A. R. Leach, *Molecular Modeling: Principles and Application*, Prentice Hall, England, 2nd edn, 2001, p. 303.
46 A. Yoshigoe and Y. Teraoka, *Surf. Sci.*, 2003, **532–535**, 690–697.
47 K.-O. Ng and D. Vanderbilt, *Phys. Rev. B: Condens. Matter Mater. Phys.*, 1999, **59**, 10132–10137.
48 A. M. Stoneham, M. A. Szymanski and A. L. Shluger, *Phys. Rev. B: Condens. Matter Mater. Phys.*, 2001, **63**, 221304.
49 G. F. Cerofolini, D. Mascolo and M. O. Vlad, *J. Appl. Phys.*, 2006, **100**, 054308.
50 D. R. Hamann, *Phys. Rev. Lett.*, 1998, **81**, 3447–3450.
51 C. C. Büttner and M. Zacharias, *Appl. Phys. Lett.*, 2006, **89**, 263106.
52 M. M. Denn, *Process Fluid Mechanics*, Prentice-Hall, Englewood Cliffs, NJ, 1980.
53 U. Khalilov, G. Pourtois, A. C. T. van Duin and E. C. Neyts, *J. Phys. Chem. C*, 2012, **116**, 8649–8656.
54 A. Korkin, J. C. Greer, G. Bersuker, V. V. Karasiev and R. J. Bartlett, *Phys. Rev. B: Condens. Matter Mater. Phys.*, 2006, **73**, 165312.
55 T.-C. Yang and K. C. Saraswat, *IEEE Trans. Electron Devices*, 2000, **47**, 746–755.
56 P. Donnadieu, E. Blanquet, N. Jakse and P. Mur, *Appl. Phys. Lett.*, 2004, **85**, 5574.